Cellular and Molecular Life Sciences (2023) 80:307
https://doi.org/10.1007/s00018-023-04955-w

ORIGINAL ARTICLE

N^4-acetylcytidine of *Nop2* mRNA is required for the transition of morula-to-blastocyst

Mengyun Wang[1] · Rui Cheng[2] · Hongjuan He[1] · Zhengbin Han[3] · Yan Zhang[4] · Qiong Wu[1]

Received: 18 April 2023 / Revised: 4 September 2023 / Accepted: 6 September 2023 / Published online: 28 September 2023

Abstract

N-acetyltransferase 10 (NAT10)-mediated N^4-acetylcytidine (ac^4C) modification is crucial for mRNA stability and translation efficiency, yet the underlying function in mammalian preimplantation embryos remains unclear. Here, we characterized the ac^4C modification landscape in mouse early embryos and found that the majority of embryos deficient in ac^4C writer-NAT10 failed to develop into normal blastocysts. Through single-cell sequencing, RNA-seq, acetylated RNA immunoprecipitation combined with PCR (acRIP-PCR), and embryonic phenotype monitoring, *Nop2* was screened as a target gene of *Nat10*. Mechanistically, *Nat10* knockdown decreases the ac^4C modification on *Nop2* mRNA and reduces RNA and protein abundance by affecting the mRNA stability of *Nop2*. Then, depletion of NOP2 may inhibit the translation of transcription factor TEAD4, resulting in defective expression of the downstream lineage-specific gene *Cdx2*, and ultimately preventing blastomeres from undergoing the trophectoderm (TE) fate. However, exogenous *Nop2* mRNA partially reverses this abnormal development. In conclusion, our findings demonstrate that defective ac^4C modification of *Nop2* mRNA hinders the morula-to-blastocyst transition by influencing the first cell fate decision in mice.

Keywords Preimplantation embryos · Development · RNA modification · Blastocyst formation · Mouse

Introduction

The process from the zygote to the blastocyst in mammals is called preimplantation embryonic development [1]. In mice, blastomeres are indistinguishable in appearance from the zygote to late 8-cell stages, but with the establishment of cell polarity and the occurrence of compaction, the blastomeres appear spatially separated for the first time, so that most blastomeres are located outside the embryo, and a few are completely enclosed inside [2, 3]. Subsequently, the embryo undergoes the first differentiation and allows the outer blastomeres to differentiate into TE, while the enclosed ones differentiate into the pluripotent inner cell mass (ICM) [4]. Previous studies have investigated the regulatory mechanisms at different developmental stages in preimplantation embryos from the perspective of histone and DNA modifications [5, 6]. Recently, it has been found that RNA modifications are also closely related to early embryonic development in vertebrates. For example, defective N6-methyladenosine (m^6A) modification inhibits oocyte maturation and zygotic genome activation (ZGA) by reducing mRNA translation efficiency and mRNA degradation in mice [7]; in zebrafish, 5-methylcytosine (m^5C) ensures the correct regulation of the maternal-to-zygotic transition (MZT) by maintaining the stability of the maternal mRNA [8]. However, other potential mechanisms of RNA modifications in the regulation of embryonic development remain to be anticipated.

Mengyun Wang, Rui Cheng have contributed equally to this work.

✉ Yan Zhang
zhangtyo@hit.edu.cn

✉ Qiong Wu
kigo@hit.edu.cn

1 Developmental Biology Laboratory, School of Life Science and Technology, Harbin Institute of Technology, Harbin 150001, China

2 Center for Bioinformatics, School of Life Science and Technology, Harbin Institute of Technology, Harbin 150001, China

3 HIT Center for Life Sciences, School of Life Science and Technology, Harbin Institute of Technology, Harbin 150001, China

4 Computational Biology Research Center, School of Life Science and Technology, Harbin Institute of Technology, Harbin 150001, China

Studies about RNA modifications can be traced back to 1960 [9], but have received widespread attention only recently due to advances in detection technology and research methods. Among conservative cytosine modifications, ac^4C modification is the only RNA acetylation event detected to date in eukaryotes; it is not only identified in tRNA and rRNA [10, 11], but also in human and yeast mRNA [12, 13]. In HeLa cells, ac^4C is mainly enriched in the coding sequences (CDS) region and gradually decreases in the 5' to 3' direction of gene transcription; it actively promotes mRNA expression and enhances translation efficiency by increasing mRNA stability [12]. Ac^4C modification is catalyzed by NAT10, a unique enzyme that shows both acetyltransferase activity and RNA-binding activity in humans [11]. Most studies that investigated NAT10-mediated ac^4C modification have focused on the occurrence and development of disease [14–18]. Just a few studies about ac^4C modification in mammalian development have been traced. For instance, *Nat10* knockdown is found to reduce ac^4C modification in mouse GV oocytes and impedes oocyte in vitro maturation [19, 20]; in addition, *Nat10* ablation of male germ cells inhibits spermatogenesis in mice [21].

In this study, we explored the effect of ac^4C modification on mouse preimplantation embryonic development. Through morphological comparisons, we found that *Nat10* was essential for the formation and maintenance of blastocysts. Intriguingly, a reduction of ac^4C modification on *Nop2* mRNA mediated by NAT10 depletion may inhibit the differentiation of blastomeres into TE cells by affecting the expression of the transcription factor CDX2, so that abnormal embryos either arrested at the morula stage or rapidly collapsed after cavitation. Together, these data reveal that NAT10-mediated ac^4C modification is crucial for morula-to-blastocyst transition in mice.

Materials and methods

Collection and in vitro culture of preimplantation embryos

Female (age 6–8 weeks) and male (age 8–12 weeks) ICR mice were purchased from the Experimental Animal Center of Harbin Medical University. Female ICR mice were intraperitoneally injected with 10 IU pregnant horse serum gonadotropin (PMSG; NSHF, China) and 10 IU human chorionic gonadotropin (hCG; NSHF, China) after a 48-h interval. Oocytes and zygotes were collected respectively from the oviducts of unmated or mated female mice 16 or 20 h after hCG injection and then treated with hyaluronidase (Sigma, H3506). Mature oocytes with the first polar body are directly used for Immunofluorescence analysis. Pronucleated zygotes were cultured in KSOM medium at 37 °C in a humidified atmosphere of 5% CO_2 until the corresponding stages.

Preparation of double-stranded RNA

DNA template was amplified from mouse zygote cDNA using primers containing the T7 promoter sequence and *Nat10* or *Nop2* exon sequences (Table S1 in Supplementary Information, primer sequences of *dsGFP* were derived from previous studies [22]). PCR products were purified using the QIAquick PCR Purification Kit (Qiagen, 28,104); then in vitro transcription was performed using the MEGAscript™ T7 Kit (Invitrogen, AM1334) according to the manufacturer's instructions. DNA template was digested with TURBO DNase, and the synthetic dsRNA was purified using phenol/chloroform (Coolaber, China). After washing with 75% ethanol, the pellet was resuspended in nuclease-free water and stored at – 80 °C.

Synthesis of siRNA

Nat10-specific siRNAs and negative control siRNA were purchased from Gene Pharma (Suzhou, China) (Table S1 in Supplementary Information), and diluted with nuclease-free water to the final concentration of 20 μM, then stored at – 80 °C.

In vitro transcription of RNA

The CDS sequences of *Nop2* and *H2B* were amplified from cDNA obtained from mouse zygotes or HeLa cells using the primers (Table S1 in Supplementary Information) and cloned into the pCS2-mCherry vector (BioVector, 936,218). The *Not I*-linearized plasmid was purified using the QIAquick PCR Purification Kit (QIAGEN, 28,104), and fusion *Nop2*- or *H2B-mCherry* RNAs were synthesized in vitro using the mMESSAGE mMACHINE SP6 (Ambion, AM1340) according to the manufacturer's instructions. The synthesized RNA was subjected to tailing reaction using the Poly (A) Tailing Kit (Ambion, AM1350) after digestion of the DNA template and purified with the MEGAclear Kit Purification for Large Scale Transcription Reactions (Ambion, AM1908).

Microinjection

The RNAs obtained by in vitro transcription were adjusted to appropriate concentrations with nuclease-free water so that the final RNA concentration for microinjection was as follows: 2.5 μg/μL for *dsGFP*/*dsNat10*, 500 ng/μL for *dsNop2*, and 100 ng/μL for *Nop2/H2B-mCherry*. Gene

knockdown experiments were performed using a piezo-micromanipulator (Prime Tech, PMAS-CT150) by injecting 5–10 pL *dsGFP*, *dsNat10*, or *dsNop2* into the cytoplasm of zygotes; in addition, single blastomeres of wild-type 2-cell embryos cultured in vitro were subjected to cytoplasmic injection with the mixture of *dsGFP/dsNop2/dsNat10* and *H2B-mCherry* 40 h after hCG injection.

For rescue experiments, *dsNat10* + *Nop2-mCherry* or *dsNat10* + *H2B-mCherry* was injected directly into zygotic cytoplasm; alternatively, cytoplasmic injection of single blastomeres with *Nop2-* or *H2B-mCherry* was performed in 2-cell embryos developed from zygotes injected with *dsNat10*. The injected embryos were cultured in vitro to the morula or blastocyst stages.

RNA-seq library construction, sequencing, and analysis

RNA-sequencing of fifty *dsGFP*- or *dsNat10*-injected morulae was performed by Beijing Genomics Institute (Shenzhen, China). The library preparation was performed following the SMARTseq2 protocol. After library construction, all samples were sequenced on the DNBSEQ platform with paired-end. The raw reads were trimmed using trim_galore. The clean reads were mapped to the mouse genome (GRCm38) using HISAT with the default parameters. The reads of each gene were counted by Htseq-count. Differentially expressed genes (DEGs) were identified by the absolute value of log2 (fold change) > 0.45.

Acquisition and analysis of publicly available datasets

The single-cell RNA-seq data of 401 embryos (48 zygotes, 48 2-cell, 73 4-cell, 142 8-cell, 64 16-cell, and 26 32-cell) were downloaded from GEO (PRJNA563325) [23]. Data processing (including preprocessing, filtering, and normalization) was carried out using the package of Seurat (version 4.0) [24]. Pearson correlation coefficient was used to calculate the expression correlation of *Nat10* and other genes at different embryonic developmental stages. Strong correlations were defined as P-value < 0.05 and absolute R > 0.45. Gene function enrichment analyses were performed by metascape [25].

RNA isolation and RT-PCR

The total RNA of F9 cells was extracted using RNAiso Plus (TaKaRa, 9109) according to the manufacturer's instructions. For preimplantation embryos, 20 zygotes, 15 2-cell, 15 4-cell, 15 8-cell, 10 morulae, or 10 blastocysts were lysed with Cells-to-signal™ kit (Ambion, AM1726) at room temperature after washing with pre-cooled PBS-PVA-DEPC. Then, the extracted total RNA of F9 cells or the embryonic lysate was reverse transcribed with PrimeScript™ RT reagent Kit (TaKaRa, RR047A). PCR amplification was performed using GoTaq Green Beat Master (Promege, M7122), and the primers are listed in Table S1.

In addition, the total RNA of 100 morulae used for acetylated RNA immunoprecipitation combined with PCR (acRIP-PCR) assay was isolated with a High Pure RNA Isolation Kit (Roach, 1,828,665) according to the manufacturer's instructions.

Immunofluorescence

According to the division of mouse embryonic age, embryonic day 0 (E 0) is defined as the moment when male and female mouse mate (usually the midpoint of the dark cycle from 7:00 pm to 5:00 am, i.e., 12:00 pm). The samples of zygotes, 2-cell, 4-cell, 8-cell, morulae, and blastocysts for immunofluorescence staining were collected at E0.5, E1.5, E2.25, E2.75, E3.5, and E4.5 (in vitro culture), respectively. After washing three times with 0.1% Triton X-100 in PBS, the samples were fixed in 4% paraformaldehyde, permeabilized in PBS supplemented with 0.5% Triton X-100, and incubated in blocking buffer (Beyotime, P0102) at room temperature. Subsequently, the embryos were incubated with ac^4C (1:500, Abcam, ab252215), NAT10 (1:1000, Abcam, ab194297), NOP2 (1:200, Proteintech, 10,448–1-AP) or TEAD4 antibody (1:200, Abcam, ab58310) overnight at 4 °C, followed by three washes with 0.1% Triton in PBS and incubated with Alexa Fluor-488 Donkey Anti-Rabbit or Mouse IgG (H + L) (1:800, Invitrogen). The DNA was stained with 4′6-diamidino-2-phenylindole (DAPI; 1:1000, Beyotime, C1002).

Counting of ICM and TE cells at the blastocyst stage was performed by counterstaining with CDX2 and DAPI. The TE cells of blocked embryos were labeled with anti-CDX2 (1:200, Biogenex, MU392A) and Alexa Fluor-546 or 488 Donkey anti-Mouse IgG (H + L) (1:800, Invitrogen). The number of ICM cells in embryos was estimated by subtracting the number of TE cells from the number of DAPI-positive cells. The fluorescence of the samples was observed using the Macro zoom fluorescence microscope (Agilent, Axio Zoom. V16).

Cell cultivation and transfection

F9 cell line was purchased from ATCC, which tested for no mycoplasma contamination, and cultured in Dulbecco′s modified Eagle′s medium (DMEM; Gibco, USA) containing 10% (v/v) fetal bovine serum (FBS; CellMax, China) and 1% Penicillin–Streptomycin Solution (Solarbio, P1400) in a humid atmosphere of 5% CO_2 at 37 °C. F9 cells were seeded

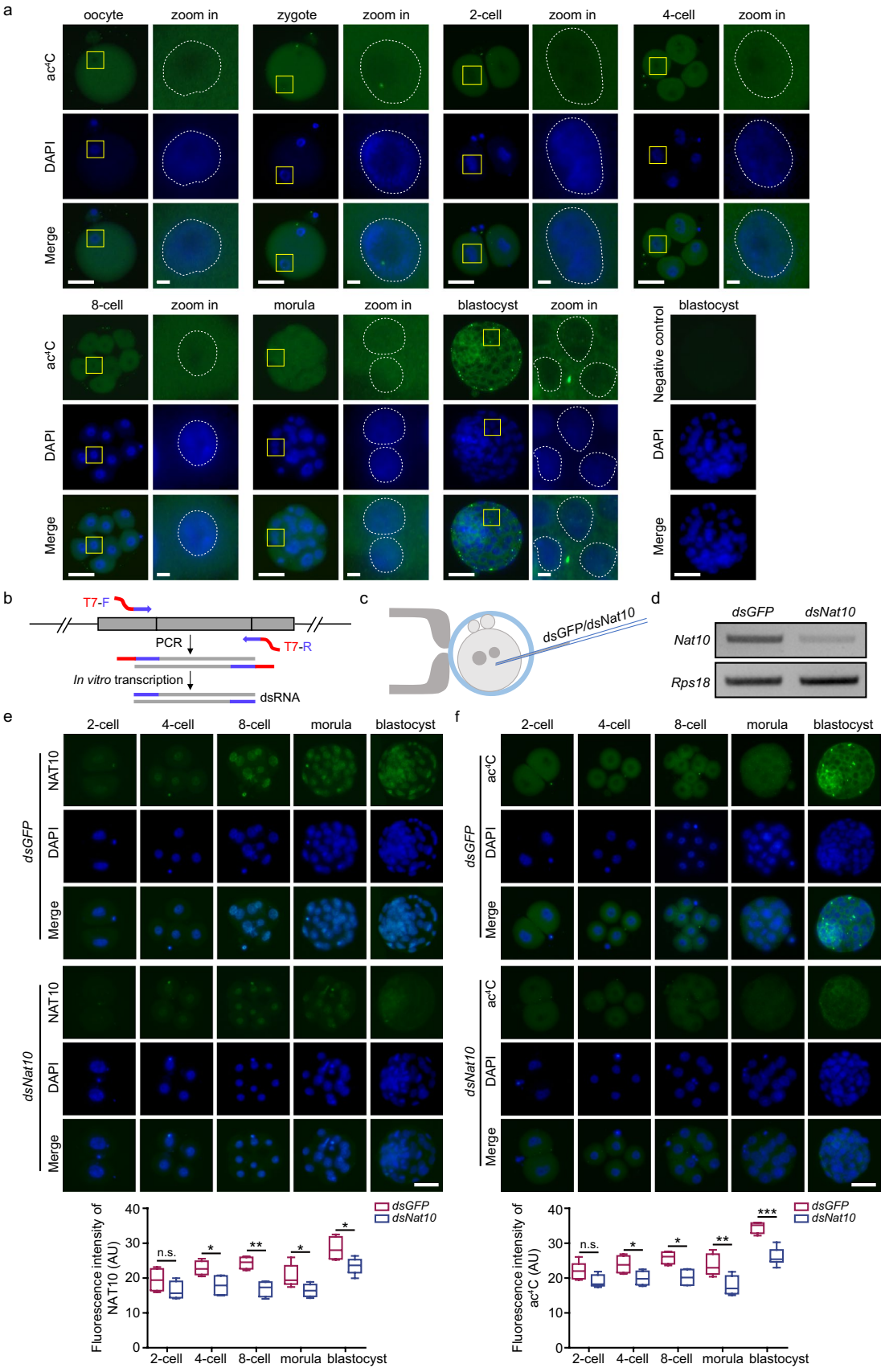
a
oocyte
zoom in
zygote
zoom in
2-cell
zoom in
4-cell
zoom in
ac4C
DAPI
Merge
8-cell
zoom in
morula
zoom in
blastocyst
zoom in
blastocyst
Negative control
DAPI
Merge
b
T7-F
PCR
T7-R
In vitro transcription
dsRNA
c
dsGFP/dsNat10
d
dsGFP
dsNat10
Nat10
Rps18
e
2-cell
4-cell
8-cell
morula
blastocyst
dsGFP
NAT10
DAPI
Merge
dsNat10
NAT10
DAPI
Merge
Fluorescence intensity of NAT10 (AU)
dsGFP
dsNat10
n.s.
*
**
*
*
2-cell
4-cell
8-cell
morula
blastocyst
f
2-cell
4-cell
8-cell
morula
blastocyst
dsGFP
ac4C
DAPI
Merge
dsNat10
ac4C
DAPI
Merge
Fluorescence intensity of ac4C (AU)
dsGFP
dsNat10
n.s.
*
*
**
***
2-cell
4-cell
8-cell
morula
blastocyst

◂**Fig. 1** Distribution of NAT10-mediated ac^4C modification in mouse preimplantation embryos. **a** Immunofluorescence staining of ac^4C (green) and DAPI (blue) in mouse oocytes ($n=7$) and preimplantation embryos (n = 8, 13, 17, 17, 15, 22 for zygote, 2-cell, 4-cell, 8-cell, morula, and blastocyst stages from three biological replicates). The yellow frames indicate the area to zoom in, and the white dotted lines indicate the boundary between the nucleus and the cytoplasm. PBS containing 0.1% Triton X-100 was used as a negative control. Scale bar, 50 μm (whole embryo) and 5 μm (zoom in). **b** Schematic diagram of dsRNA preparation. Gray rectangles, purple thick lines, and red thick lines indicate exons, gene-specific primers, and T7 promoter sequences, respectively. **c** Schematic diagram of cytoplasmic microinjection in zygote. The final injection concentration of *dsGFP* or *dsNat10* is 2.5 μg/μL. **d** RT-PCR verification of *dsNat10* knockdown efficiency in morulae. *dsGFP* as the negative control. **e**, **f** Immunofluorescence analysis of NAT10 (**e**) or ac^4C (**f**) in *Nat10*-depleted preimplantation embryos (n = 15 for each group from three biological replicates). The fluorescence intensity (mean) was calculated by the ratio of Integrated Density to Area. Scale bar, 50 μm. Boxplots showing the fluorescence intensity of NAT10 (**e**) or ac^4C (**f**) in dsRNA-injected preimplantation embryos, respectively. The middle lines indicate the median, and the boxes indicate the 25th/75th percentiles. $^*P<0.05$; $^{**}P<0.01$; $^{***}P<0.001$; *n.s.* no significance (two-sided Student′s *t*-test). AU arbitrary units

in 24-well plates and transfected with siRNA (20 pmol) using Lipofectamine 3000 (Invitrogen, L3000015) when cells reached 50–60% confluence. Then, total RNA was isolated after 48 h of incubation.

acRIP-PCR

acRIP assays for F9 cells or morulae total RNA were performed according to the protocol of Magna MeRIP™ m6A Kit (Millipore, 17–10,499) and the previous description [26] with some improvement as follows.

RNA fragmentation. Either 100 morulae or 10 μg F9 cells total RNA was diluted to 18 μL with nuclease-free water in a PCR tube. Then, 2 μL 10 × Fragmentation buffer was added, and the sample was incubated at 94 °C for 4 min. The fragmentation reactions were terminated by adding 2 μL 0.5 M EDTA and vortexing.

Purification of fragmented RNA Fragmented RNA was transferred to a 1.5 mL RNase-free tube and diluted to 200 μL with nuclease-free water. An equal volume of phenol/chloroform was added, and the sample was mixed thoroughly and centrifuged at full speed. The aqueous phase was transferred to a new tube, and an equal volume of chloroform was added; the aqueous phase was transferred to a new tube again after centrifuging. Linear acrylamide solution (Sangon Biotech, A610548) and ethanol were added for RNA precipitation. Then, the fragmented RNA was centrifuged at full speed, washed with 75% ethanol, and dissolved in nuclease-free water.

Preparation of magnetic beads Magna ChIP Protein A/G Magnetic Beads were washed and resuspended in 1 × IP buffer. Then, 0.5 μg anti-ac^4C (Abcam, ab252215) or anti-IgG was added and incubated at room temperature for 30 min. The supernatant was removed followed by three washes with 1 × IP buffer.

Immunoprecipitation Most of the fragmented RNA was mixed with 5 × IP buffer, nuclease-free water, and RNase inhibitor to prepare an RIP reaction mixture. The mixture was divided into two equal parts and rotated with magnetic beads coated with anti-ac^4C or IgG at 4 °C for 2 h. A 1/10 volume of the RNA for immunoprecipitation was treated as "input". The RNA/antibody-coated beads were washed three times with 1 × IP buffer after immunoprecipitation.

Elution The RNA/antibody-coated beads were resuspended in 1 × Protease K buffer containing 100 mM Tris–HCl (pH 7.5), 150 mM NaCl, 12.5 mM EDTA, 2% SDS, and 5 mg/mL proteinase K, and incubated at 37 °C for 30 min. The supernatant was transferred to a new RNase-free tube, and then an equal volume of phenol/chloroform was added to purify the RNA as described above.

RT-PCR. The purified RNA was immediately reverse-transcribed as described above. Then, the corresponding primers of *Nop2*-1 and *Nop2*-2 were used for PCR amplification (Table S1 in Supporting Information). The enrichment of ac^4C in each RIP group was normalized according to the results of the input group.

Dual-Luciferase reporter assay

The CDS sequence of *Nop2* mRNA containing wild-type potential ac^4C modification sites was amplified from the cDNA of F9 cells and inserted into the multiple cloning site (MCS) at the downstream of the Firefly luciferase gene driven by the CMV promoter in pMIR-Report to construct the fusion vector of Firefly luciferase gene and *Nop2* CDS sequence: pMIR-Report-*Nop2* WT. The vectors with mutant ac^4C sites, including pMIR-Report-*Nop2* Mut 1, pMIR-Report-*Nop2* Mut 2, and pMIR-Report-*Nop2* Mut 1 + 2, were obtained using the KOD-Plus-Mutagenesis Kit (TOYOBO, SMK-101). Then, the WT or Mut vector and Renilla luciferase reporter vector were co-transfected into F9 cells 24 h after siRNA transfection. The dual-luciferase reporter assay was performed after 48 h using the Dual-Luciferase® Reporter Assay System (Progema, E1910) according to the manufacturer's instructions, and the relative luciferase activity was calculated by the ratio of Firefly luciferase activity to Renilla luciferase activity.

mRNA stability assay

F9 cells were seeded in 24-well plates and transfected with *si-Nat10* or *si-NC*. After 48 h, cell samples were treated with 5 μg/mL actinomycin D (ActD, Sigma) for 0 h, 3 h, and 6 h. For preimplantation embryos, the morulae (at E3.5) derived from zygotes injected with *dsGFP* or *dsNat10* were transferred to KSOM medium containing ActD (5 μg/mL) and incubated

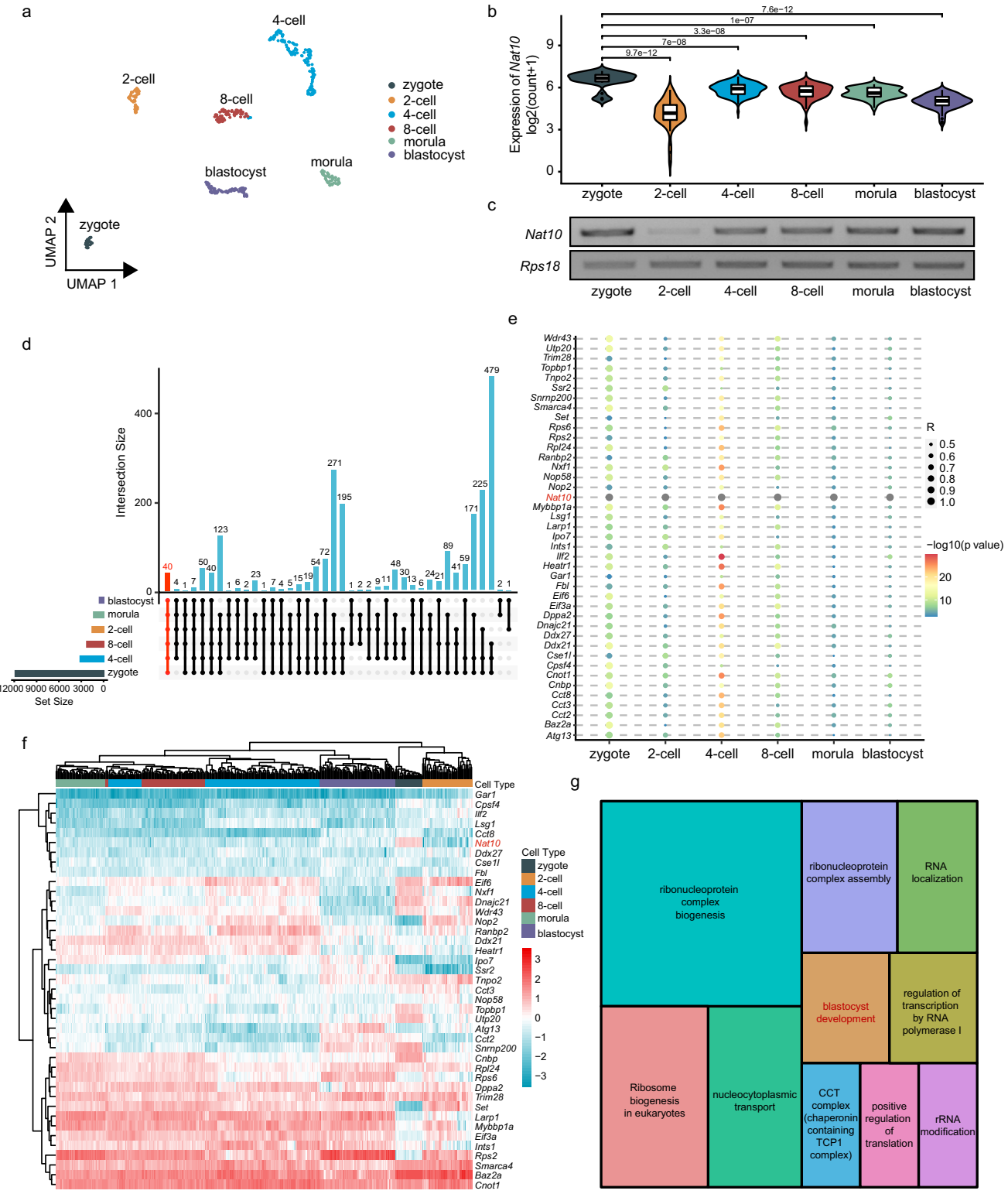

for 0 h, 3 h, and 6 h. Then, RNA extraction and cDNA synthesis were performed as described above. The expression of genes was analyzed by qRT-PCR and normalized to *GAPDH*, and the degradation rate of mRNA was calculated according to published protocols[27].

Statistics

Statistical analyses were performed using GraphPad Prism (GraphPad Corp.) and Excel software (MicroSoft Corp.). All experiments were repeated three times at least, and the data

◂**Fig. 2** *Nat10* is involved in blastocyst formation in mice. **a** UMAP projection of single-cell RNA sequencing for mouse preimplantation embryos. Each dot corresponds to one blastomere and is colored according to developmental stage. **b** Violin plot showing the differential expression of *Nat10* from the zygote to blastocyst stages. **c** RT-PCR analysis of *Nat10* in different developmental stages of preimplantation embryos. **d** Upset plot showing the distribution of genes correlated with *Nat10* expression, 40 of which intersect at six developmental periods. **e** Bubble plot indicating the genes strongly correlated with *Nat10*. The size and color of each bubble correspond to correlations and -log10 (P value), respectively. **f** Hierarchical clustering of the genes correlated with *Nat10*. **g** Treemap of condensed gene ontology (GO) terms for *Nat10*-correlated genes. The size of each box indicates the number of significant terms associated with the GO category

was presented as mean ± SEM. The two-sided Student′s *t*-test was used for pairwise comparisons, and the one-way ANOVA was applied for multiple group comparisons. Specifically, the value of $P < 0.05$, $P < 0.01$, or $P < 0.001$ was considered a significant difference (*, $P < 0.05$; **, $P < 0.01$; ***, $P < 0.001$; different letters between a and b, $P < 0.05$; different letters between A and B, $p < 0.01$).

Results

Dynamic change of NAT10-mediated ac^{4}C modification during preimplantation embryonic development

To characterize whether preimplantation embryonic development in mice involves ac^{4}C modification, immunofluorescence staining (IF) was performed. The results showed that the ac^{4}C signal was detected in the cytoplasm and nucleus of preimplantation embryos (Fig. 1a). At present, NAT10 is a unique human writing protein of ac^{4}C [11, 12]. To further confirm that the modification of ac^{4}C in mouse preimplantation embryos is also mediated by NAT10, we injected *Nat10*-specific double-stranded RNA (dsRNA, an RNA molecule that can be processed into siRNAs by Dicer and then mediate specific gene silencing) into the cytoplasm of zygotes; *dsGFP*-injected embryos served as the control (Fig. 1b, c). The localization and signal intensity of NAT10 and ac^{4}C from the 2-cell to blastocyst stages were detected after verifying knockdown efficiency at the morula stage (Fig. 1d). Slightly different from the distribution of ac^{4}C, NAT10 was mainly localized in the nucleus, with lower levels at the early stages (Fig. 1e). The acetyltransferase NAT10 catalyzes the acetylation of specific cytosine nucleosides in mRNAs, therefore, the signals of ac^{4}C modification could be detected in the nucleus. However, mature mRNAs are translated into proteins in the cytoplasm; on the other hand, although current studies have not yet identified the ac^{4}C-binding proteins, the ac^{4}C modification of mRNA may be similar to m^{6}A, which plays different roles through the recognition of different readers in the cytoplasm[28, 29], making the signal of ac^{4}C modification in the cytoplasm clearer. The abundance of NAT10 increased from the 4-cell stage, which was consistent with the signal of ac^{4}C modification. In addition, *dsNat10* significantly inhibited the level of NAT10. Concomitant with this downregulation, the global modification of ac^{4}C in embryos at the same stages was attenuated, especially at the morula and blastocyst stages (Fig. 1f), indicating that ac^{4}C is also mediated by NAT10 in mouse preimplantation embryos.

Nat10 is involved in blastocyst development

Single-cell RNA sequencing data were obtained from the GEO database (PRJNA563325) [23] and used to analyze the potential effects of *Nat10* during preimplantation embryonic development. Clusters of diverse development stages were visualized using Uniform Manifold Approximation and Projection (UMAP) (Fig. 2a). The level of *Nat10* expression peaked at the zygote stage and showed a trend of first decreasing and then increasing in response to maternal RNA degradation and ZGA (Fig. 2b, c). It is worth noting that among the genes correlated with *Nat10* expression, 40 were strongly correlated with *Nat10* at each developmental stage (Fig. 2d, e). We further performed cluster analysis on the expression of these 40 genes, and the results showed that the expression of these genes was mostly different (Fig. 2f). Functional enrichment revealed that these 40 genes are involved in ribonucleoprotein complex biogenesis, ribosome biogenesis in eukaryotes, positive regulation of translation, and blastocyst development (Fig. 2g).

Nat10 depletion arrests the morula-to-blastocyst transition

To confirm the effect of *Nat10* on preimplantation embryonic development, we monitored the developmental potential of non-injected embryos as well as the ones injected with *dsGFP* or *dsNat10* at the zygote stage. From the 2-cell to morula stages, there were no differences in morphology or embryogenesis rate among the three groups (Fig. 3a, b; Fig. S1a). However, the blastocyst formation rate was significantly lower at E4.5 in the *dsNat10*-injected group (45.05 ± 6.88%) than in others (non-injection, 89.33 ± 4.52%; *dsGFP*-injected group, 86.00 ± 5.21%) (Fig. 3a, c; Fig. S1c). Subsequently, the blastocysts of two control groups continued to expand and mostly hatched from the zona pellucida; in contrast, the majority of *Nat10*-depleted blastocysts exhibited cavity collapse and retraction, while the

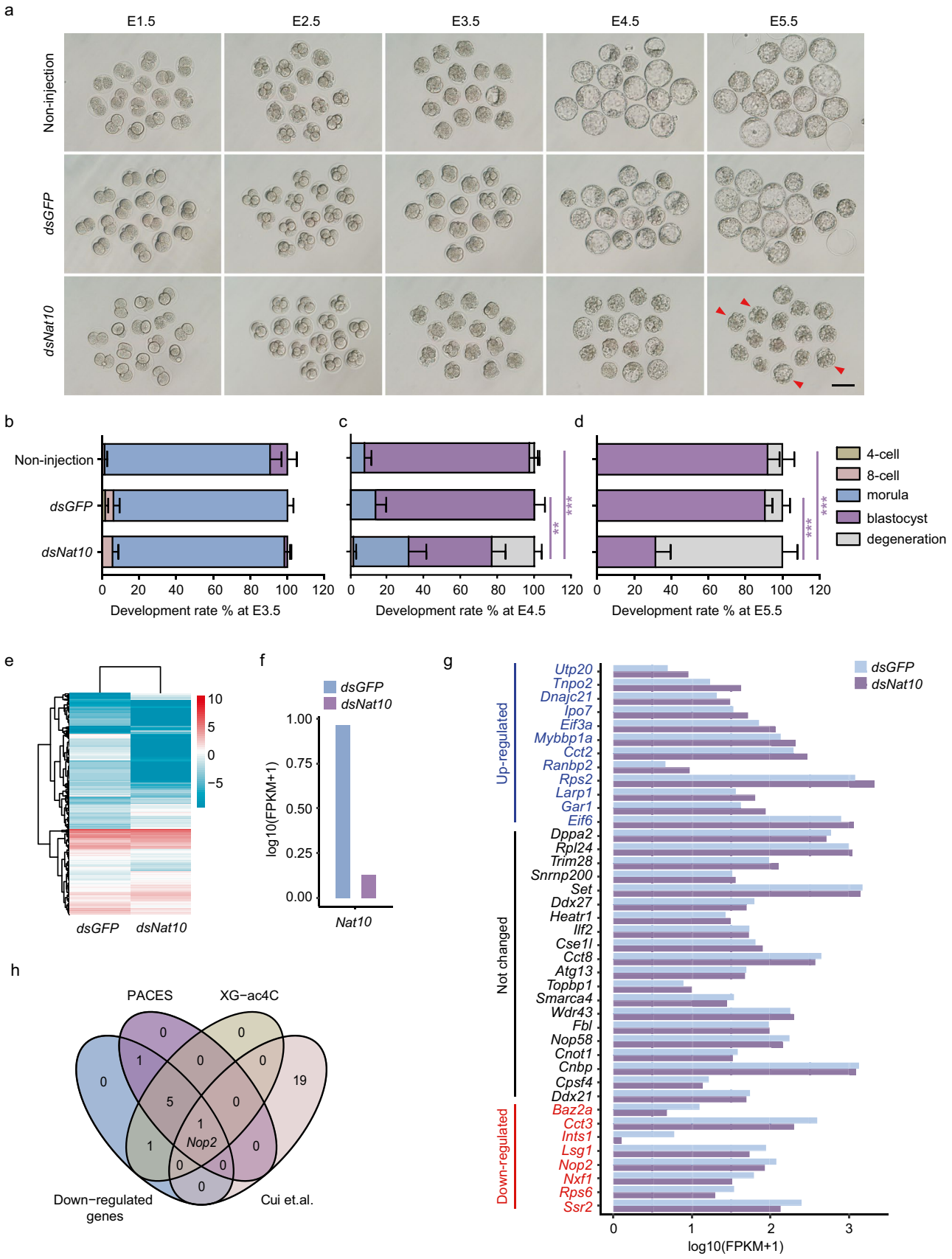
a
E1.5
E2.5
E3.5
E4.5
E5.5
Non-injection
dsGFP
dsNat10
b
c
d
Non-injection
dsGFP
dsNat10
0 20 40 60 80 100 120
Development rate % at E3.5
Development rate % at E4.5
Development rate % at E5.5
**
***
4-cell
8-cell
morula
blastocyst
degeneration
e
10
5
0
−5
dsGFP
dsNat10
f
dsGFP
dsNat10
log10(FPKM+1)
1.00
0.75
0.50
0.25
0.00
Nat10
g
dsGFP
dsNat10
Up-regulated
Not changed
Down-regulated
Utp20
Tnpo2
Dnajc21
Ipo7
Eif3a
Mybbp1a
Cct2
Ranbp2
Rps2
Larp1
Gar1
Eif6
Dppa2
Rpl24
Trim28
Snrnp200
Set
Ddx27
Heatr1
Ilf2
Cse1l
Cct8
Atg13
Topbp1
Smarca4
Wdr43
Fbl
Nop58
Cnot1
Cnbp
Cpsf4
Ddx21
Baz2a
Cct3
Ints1
Lsg1
Nop2
Nxf1
Rps6
Ssr2
0 1 2 3
log10(FPKM+1)
h
PACES
XG−ac4C
Down−regulated genes
Cui et.al.
0
0
1
0
0
0
5
0
19
1
Nop2
1
0
0
0
0

◂**Fig. 3** *Nat10* depletion arrests morula-to-blastocyst transition. **a** Representative images of preimplantation embryos in the non-injection, *dsGFP*-, and *dsNat10*-injected groups (five biological replicates). Red arrowheads denote degenerating blastocysts. Scale bar, 100 μm. **b–d** Statistics of development rate among the three groups. There was no difference in embryo development at E3.5 (**b**), but the blastocyst formation rate of *Nat10*-depleted embryos was significantly reduced at E4.5 (**c**) and E5.5 (**d**). Error bars indicate the SEM in five biological replicates. $^{**}p < 0.01$; $^{***}p < 0.001$ (one-way ANOVA). **e** Heatmap showing the DEGs between *dsGFP*- and *dsNat10*-injected morulae. **f** The expression of *Nat10* in RNA-Seq data. **g** Bar plot presenting the expression changes of 40 genes correlated with *Nat10* expression in *Nat10*-depleted morulae. **h** Four-way Venn diagram for screening the potential target genes of *Nat10*. Down-regulated genes, the 8 genes in (**g**); PACES, the number of potential ac^{4}C modification genes predicted by PACES software (among 8 down-regulated genes); XG-ac4C, the number of potential ac^{4}C modification genes predicted by XG-ac4C software (among 8 down-regulated genes); Cui et al., 20 genes that are necessary for mouse blastocyst formation [22]

remaining embryos arrested and degenerated before blastocyst cavitation (Fig. 3a, d; Fig. S1b). Therefore, we ruled out the possibility that the depletion of *Nat10* could delay embryonic development. In addition, zygotes were injected with *si-NC* or two siRNAs designed against *Nat10* to further confirm that the abnormality of blastocyst formation caused by *dsNat10* is not related to the depletion of non-specific genes (Fig. S1d–f).

Fifty morulae derived from zygotes injected with *dsGFP* or *dsNat10* were collected at E3.5 for RNA sequencing to investigate the underlying mechanisms of failed embryonic development. According to the absolute value of log2(fold change) > 0.45, a total of 8825 DEGs were detected between two groups, of which 3506 were up-regulated and 5319 were down-regulated in the *dsNat10*-injected group (Fig. 3e, Table S2). Moreover, compared with the *dsGFP*-injected group, *dsNat10* decreased the expression level of *Nat10* in morulae (Fig. 3f), which was consistent with the RT-PCR (Fig. 1d). Since ac^{4}C modification contributes to maintaining the stability of mRNA, we were more inclined to screen down-regulated DEGs as candidate target genes. Based on the above single-cell RNA sequencing results (Fig. 2d, e), 40 genes strongly correlated with *Nat10* expression at all preimplantation stages were screened, and 8 genes (*Baz2a*, *Cct3*, *Ints1*, *Lsg1*, *Nop2*, *Nxf1*, *Rps6*, and *Ssr2*) among them were downregulated in *dsNat10*-injected morulae (Fig. 3g). To estimate whether the candidate genes were modified by ac^{4}C, we used PACES and XG-ac4C software to predict the potential ac^{4}C sites of these genes, and the results showed that ac^{4}C modification may exist in the 5'UTR, CDS and/or 3'UTR regions of *Baz2a*, *Ints1*, *Lsg1, Nop2*, *Nxf1*, and *Ssr2* mRNA (Fig. S2). Among the 20 genes reported to be essential for mouse blastocyst formation [22], we were pleasantly surprised to find *Nop2* (Fig. 3h). Thus, further detection was performed to verify the potential targeting relationship between *Nop2* and *Nat10*.

NAT10 regulates ac^{4}C modification of *Nop2* mRNA in morulae

The prediction results of PACES revealed that the CDS region of *Nop2* mRNA contains two ac^{4}C modification sites, and we labeled them *Nop2*-1 and *Nop2*-2 according to the sequence from 5′ to 3′ (Fig. 4a). To evaluate the effect of *Nat10* on *Nop2* gene regulation, we first transfected the siRNA to knockdown *Nat10* in F9 cells. The results showed that *Nop2* expression was decreased after *Nat10* depletion (Fig. 4b). Then, luciferase reporter vectors with two wild-type sites (pMIR-Report-*Nop2* WT), single- or double-mutation sites (pMIR-Report-*Nop2* Mut 1, pMIR-Report-*Nop2* Mut 2, or pMIR-Report-*Nop2* Mut 1 + 2) were constructed for dual-luciferase reporter assay (Fig. 4c). In F9 cells transfected with the luciferase reporter vector containing either wild-type or single-mutation of ac^{4}C potential modification sites, *Nat10* depletion mediated by siRNA reduced the relative luciferase activity (Fig. 4d). It is worth noting that in cells transfected with negative control siRNA, the relative luciferase activity of the pMIR-Report-*Nop2* Mut 2 group was slightly lower than that of the WT and Mut 1 groups; however, there was no change of the relative luciferase activity in *Nat10*-depleted F9 cells from three groups, indicating that *Nop2*-1 may be less affected by *Nat10* than the *Nop2*-2 site. In cells transfected with the vector containing the double-mutation sites, the relative luciferase activity did not decrease with *Nat10* knockdown; on the other hand, the relative luciferase activity of the pMIR-Report-*Nop2* Mut 1 + 2 group was still lower than that of the WT group in control F9 cells. These results further suggested that both potential ac^{4}C modification sites in the *Nop2* CDS region are affected by *Nat10* expression. In addition, F9 cells or morulae were treated with ActD, a transcription inhibitor, and the expression of *Nop2* was detected through qRT-PCR to investigate whether the mRNA stability of *Nop2* is regulated by *Nat10*. When samples were treated with ActD for various lengths of time, the detectable mRNAs corresponded to the portion that had not yet degraded. As shown in Fig. 4e, f, *Nat10* depletion shortened the half-life of *Nop2* mRNA in F9 cells and morulae. In mouse oocytes, ac^{4}C modification mediated by NAT10 actively maintained mRNA expression by inhibiting mRNA degradation. Thus, the above data indicate that *Nat10* regulates the expression of *Nop2* by affecting the mRNA stability.

Furthermore, to verify whether the regulation of *Nat10* on *Nop2* is mediated by ac^{4}C modification, acRIP-PCR was performed on both F9 cells and mouse morulae (Fig. 4g). DNA fragments containing *Nop2*-1 or *Nop2*-2 site could be amplified in F9 cells (Fig. 4h, left), indicating that both predicted sites in the CDS region of *Nop2* mRNA

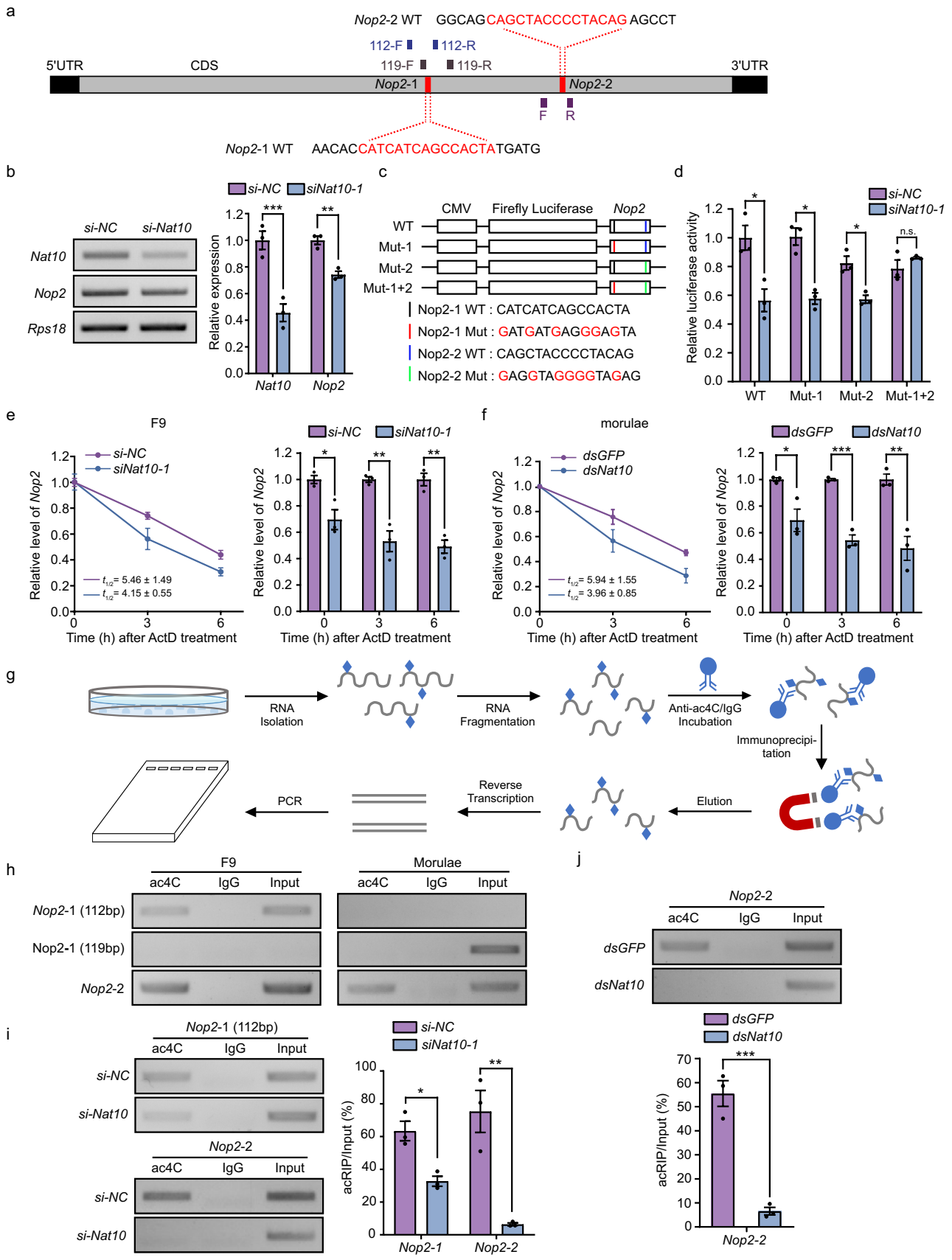
a
Nop2-2 WT GGCAGCAGCTACCCCTACAG AGCCT
112-F 112-R
5'UTR CDS 119-F 119-R 3'UTR
Nop2-1 Nop2-2
F R
Nop2-1 WT AACACCATCATCAGCCACTATGATG
b
si-NC si-Nat10
Nat10
Nop2
Rps18
si-NC siNat10-1
Relative expression
Nat10 Nop2
c
CMV Firefly Luciferase Nop2
WT
Mut-1
Mut-2
Mut-1+2
Nop2-1 WT : CATCATCAGCCACTA
Nop2-1 Mut : GATGATGAGGGAGTA
Nop2-2 WT : CAGCTACCCCTACAG
Nop2-2 Mut : GAGGTAGGGGTAGAG
d
si-NC siNat10-1
Relative luciferase activity
n.s.
WT Mut-1 Mut-2 Mut-1+2
e
F9
si-NC siNat10-1
Relative level of Nop2
t1/2= 5.46 ± 1.49
t1/2= 4.15 ± 0.55
Time (h) after ActD treatment
f
morulae
dsGFP dsNat10
t1/2= 5.94 ± 1.55
t1/2= 3.96 ± 0.85
g
RNA Isolation
RNA Fragmentation
Anti-ac4C/IgG Incubation
Immunoprecipi-tation
Elution
Reverse Transcription
PCR
h
F9
Morulae
ac4C IgG Input
Nop2-1 (112bp)
Nop2-1 (119bp)
Nop2-2
j
Nop2-2
ac4C IgG Input
dsGFP
dsNat10
acRIP/Input (%)
i
Nop2-1 (112bp)
ac4C IgG Input
si-NC
si-Nat10
Nop2-2
Nop2-1 Nop2-2

◂**Fig. 4** *Nop2* is a target gene of *Nat10* in mouse preimplantation embryos. **a** Potential sites for ac^4C modification in mouse *Nop2* mRNA, which were named *Nop2*-1 and *Nop2*-2 in sequence from 5' to 3'. Gray and black rectangles indicate the CDS and UTRs of *Nop2*, respectively. The colored bold vertical lines represent the primers of acRIP-PCR. **b** RT-PCR analyses of *Nat10* and *Nop2* in F9 cells transfected with siRNA. The RT-PCR data were normalized to the expression of *Rps18*. **c** Schematic presentation of the pMIR-Report luciferase reporters containing wild type and mutant CDS of *Nop2* mRNA. WT, wide-type; Mut, mutation. **d** Wild-type or mutant ac^4C sites were cloned into a pMIR-Report vector and transfected into siRNA-treated F9 cells to perform dual-luciferase reporter assays. Firefly luciferase activity was measured and normalized to that of Renilla luciferase activity. **e–f** The mRNA stability and expression of *Nop2* were detected by qRT-PCR in F9 cells (**e**) or morulae (**f**) treated with 5 μg/mL ActD. **g** Flow chart of acRIP-PCR. **h** Detection of ac^4C modification sites on *Nop2* mRNA in wild-type F9 cells and mouse morulae. **i-j** NAT10-mediated ac^4C modification in *Nop2* mRNA in F9 cells (**i**) and mouse morulae (**j**) was confirmed by acRIP-PCR. The enrichment of ac^4C in each RIP group was normalized according to the results of the input group. For **b, d–f**, **i**,and **j**, error bars indicate the SEM in three biological replicates. $^*P < 0.05$; $^{**}P < 0.01$; $^{***}P < 0.001$; *n.s.* no significance (two-sided Student's *t*-test)

are modified by ac^4C, consistent with the results of the dual-luciferase reporter assay. In morulae, only the *Nop2*-2 site could be detected when we used the same primers as F9 cells for PCR amplification. This was due to the fact the amount of total RNA in morulae used for acRIP-PCR was considerably lower than that of F9 cells, resulting in different sizes of RNA fragments after fragmentation. Therefore, we substituted the primers of *Nop2*-1 and successfully amplified a 119 bp target fragment in the input group rather than the ac^4C group (Fig. 4h, right). The tissue-specificity and motif bias of the ac^4C modification on mRNA may be the reason for the difference in acRIP-PCR assay between F9 cells and morulae. Subsequently, the total RNA of F9 cells and morulae was utilized to investigate the acetylation modification of *Nop2* upon *Nat10* depletion. As predicted, ac^4C modification in *Nop2* mRNA was significantly decreased with the reduction of *Nat10* expression (Fig. 4i, j). Taken together, the above-pooled results strongly suggest that *Nat10* regulates *Nop2* gene expression through ac^4C modification in mouse morulae.

NAT10 affects the morula-to-blastocyst transition by regulating NOP2

To confirm the *Nat10-Nop2* regulatory role, we first examined the effect of *Nat10* on *Nop2* expression. Similar to *Nat10*, the mRNA abundance of *Nop2* showed dynamic changes at various preimplantation periods (Fig. S3a, b) and decreased in *Nat10*-depleted embryos (Fig. S3c–g), especially at the morula stage. NOP2 protein was distributed in the nucleolus, nucleoplasm, and cytoplasm from the 2-cell to 8-cell stages (Fig. 5a–c; Fig. S4a–c), but mainly localized in the nucleolus of morulae and blastocysts (Fig. 5d, e; Fig. S4d, e). Notably, the NOP2 signal was significantly reduced in *Nat10*-depleted embryos, especially in the nucleus, indicating that NAT10 is involved in the regulation of NOP2 protein abundance through the effect on the Nop2 expression.

Further, after screening the injection concentration (Fig. S3h), we injected *Nop2*-specific dsRNA into the cytoplasm of zygotes and tracked the embryonic development. The results demonstrated that *Nop2*-depleted preimplantation embryos were mostly arrested at the morula stage, which was comparable to *dsNat10*-injected embryos (Fig. 5f). Thus, a fused *Nop2-mCherry* RNA was synthesized in vitro and used in rescue experiments for *Nat10*-depleted embryos. RT-PCR indicated that *Nop2-mCherry* significantly increased the RNA level of *Nop2* in *Nat10*-depleted morulae (Fig. 5g). On the other hand, exogenous *Nop2* RNA enhanced the potential of abnormal embryos to transform into blastocysts to a certain extent, although blastocyst development delayed (Fig. 5h, i; Fig. S1b, c).

Depletion of *Nop2* mediated by NAT10 knockdown prevents blastomeres from undergoing the TE fate

Previous studies have shown that CDX2 is involved in the formation and maintenance of TE cells [30, 31]. To test the hypothesis that the inhibition of blastocyst formation in *Nat10*-depleted embryos may be related to the abnormal expression of CDX2 mediated by NOP2, IF was performed for *Nat10*- or *Nop2*-depleted morulae and non-collapsed blastocysts. We found that the signal of CDX2 was significantly weakened in the embryos derived from zygotes injected with *dsNat10* or *dsNop2* (Fig. 6a), indicating that the aberrant development of *Nat10*-depleted embryos was accompanied by a decrease in CDX2 abundance. TEAD4 is considered an important transcription factor that regulates *Cdx2* during preimplantation development in mice [32, 33]. Therefore, IF analyses of TEAD4 were further performed, and the results confirmed that the TEAD4 protein was strongly suppressed in *Nat10*- or *Nop2*-depleted embryos (Fig. 6b).

Additionally, we noticed that the number of total cells and TE cells in *Nat10*- and *Nop2*-depleted blastocysts were significantly lower than in the control group; although the difference was not significant, the number of ICM cells was slightly reduced and the ratio of ICM to TE cells was marginally elevated (Fig. 6c), suggesting that NAT10 may also influence the first cell fate decision by regulating *Nop2*. Thus, random single blastomeres of 2-cell embryos were injected with dsRNA and *H2B-mCherry* (Fig. 6d). The abundance of CDX2 protein was reduced in the cells developed from blastomeres injected with a mixture of *dsNat10* and *H2B-mCherry*, or *dsNop2* and *H2B-mCherry* (Fig. 6e; Fig. S5a), and the number of total cells and TE cells in

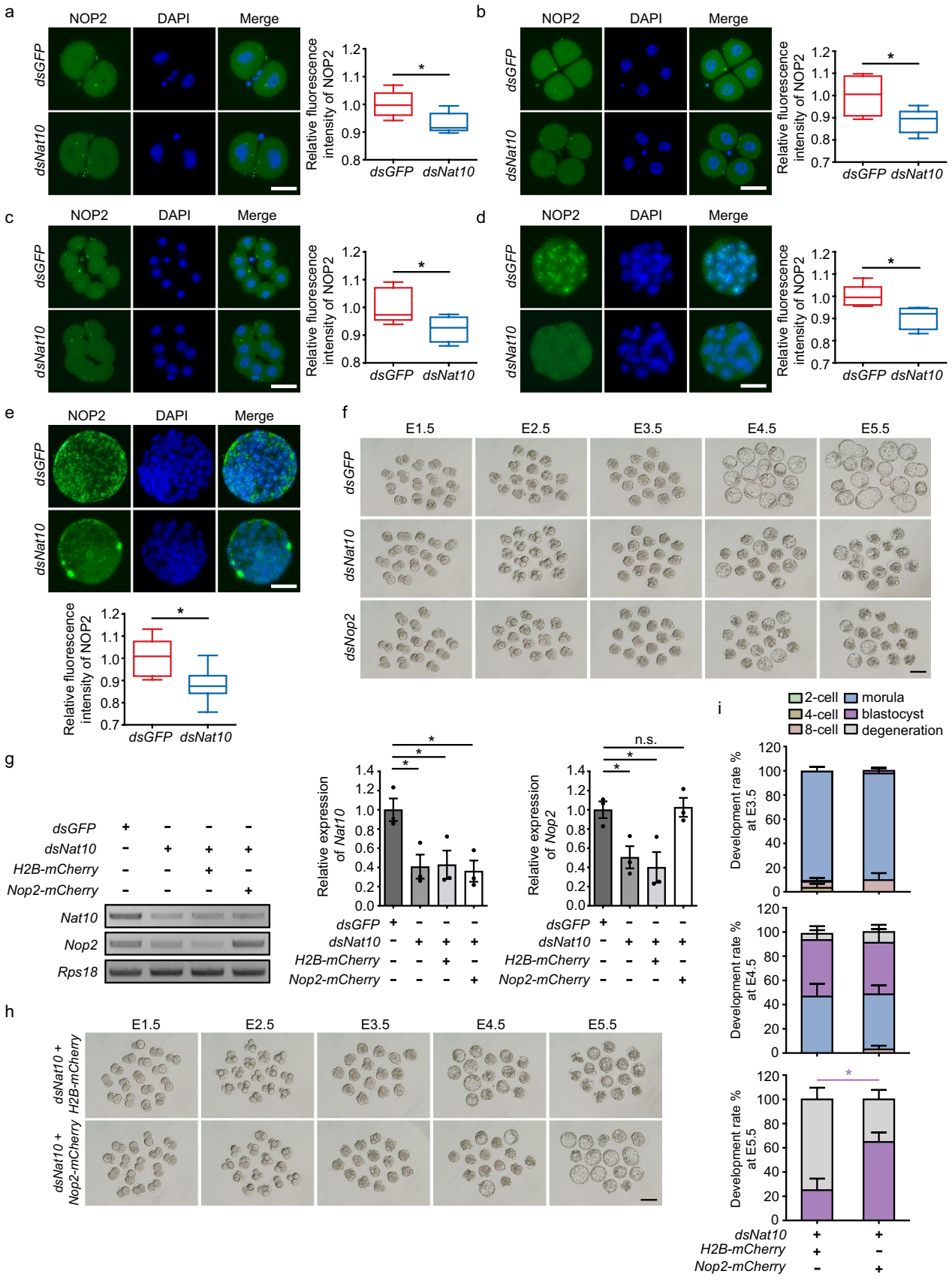
a
NOP2
DAPI
Merge
dsGFP
dsNat10
Relative fluorescence intensity of NOP2
dsGFP dsNat10
b
c
d
e
f
E1.5
E2.5
E3.5
E4.5
E5.5
dsNop2
g
dsGFP
dsNat10
H2B-mCherry
Nop2-mCherry
Nat10
Nop2
Rps18
Relative expression of Nat10
Relative expression of Nop2
n.s.
h
dsNat10 + H2B-mCherry
dsNat10 + Nop2-mCherry
i
2-cell
4-cell
8-cell
morula
blastocyst
degeneration
Development rate % at E3.5
Development rate % at E4.5
Development rate % at E5.5

◂**Fig. 5** *Nop2* partially reverses morula arrest caused by *Nat10* depletion. **a–e** Immunofluorescence analysis of NOP2 in 2-cell (**a**), 4-cell (**b**), 8-cell (**c**), morulae (**d**), and blastocysts (**e**) derived from zygotes injected with dsRNA (n = 15 for each group from three biological replicates). Scale bar, 50 μm. Boxplot charts showing the effect of *Nat10* depletion on the expression of NOP2 protein in preimplantation embryos. The mean fluorescence intensity in *dsNat10*-injected embryos was measured and normalized to the mean fluorescence intensity in *dsGFP*-injected embryos. The middle lines indicate the median, and the boxes indicate the 25th/75th percentiles. $*P < 0.05$. **f** Representative images of preimplantation embryos injected with *dsGFP*, *dsNat10*, or *dsNop2* from E1.5 to E5.5 (three biological replicates). Similar to *Nat10* knockdown, most *Nop2*-depleted embryos are arrested at the morula stage. Scale bar, 100 μm. **g** RT-PCR results confirmed that exogenous *Nop2* RNA increased *Nop2* mRNA in *Nat10*-depleted morulae. The relative expression was normalized to the expression of *Rps18*. **h** Representative images of rescue with exogenous *Nop2* RNA for abnormal development caused by *Nat10* depletion. Scale bar, 100 μm. **i** Statistics of development rate. There were no differences in the developmental potential of embryos between the groups at E3.5 or E4.5; but at E5.5, the blastocyst formation rate of *Nat10*-depleted embryos was significantly increased after *Nop2* RNA co-injection. For **g** and **i**, error bars indicate the SEM in three biological replicates. *P* values were determined by one-way ANOVA (**g**) or two-sided Student′s *t*-test (**i**). $*p < 0.05$; *n.s.* no significance

blastocysts was significantly decreased compared to blastomeres injected with *dsGFP* and *H2B-mCherry* (Fig. 6f), which was similar to the cytoplasmic injection of zygotes (Fig. 6c). On the other hand, in embryos injected with *dsNat10* or *dsNop2*, the contribution of mCherry-positive blastomeres to TE was significantly reduced, while the contribution to ICM was not significantly changed (Fig. 6g; Fig. S5b), indicating that *Nat10* depletion prevents blastomeres from undergoing the TE fate.

Exogenous *Nop2* biases *Nat10*-depleted blastomeres toward the TE fate

We next explored the effect of *Nop2* on cell fate determination in *Nat10*-depleted embryos. *Nop2-mCherry* RNA was injected into random single blastomeres of 2-cell embryos derived from *dsNat10*-injected zygotes (Fig. 7a). As expected, *Nop2-mCherry* increased the expression of CDX2 compared to cells derived from blastomeres that were not injected or injected with *H2B-mCherry* (Fig. 7b, c; Fig. S6a). Moreover, exogenous *Nop2* increased the number of total cells and TE cells in blastocysts (Fig. 7d) and promoted the development of mCherry-positive blastomeres into TE cells but had no significant influence on ICM development (Fig. 7e; Fig. S6b). Together, our data verify that the downregulation of *Nop2* mRNA mediated by *Nat10* depletion affects the expression of CDX2 and ultimately leads to aberrant first-cell fate decision.

As a transcription factor involved in the first cell fate determination in mice, TEAD4 binds to YAP1, which is transported from the cytoplasm to the nucleus, to initiate the expression of downstream genes *Cdx2* and *Gata3*. RT-PCR results showed that the amounts of *Cdx2* and *Gata3* mRNA in *Nat10*-depleted morulae were both reduced (Fig. 7f), suggesting abnormal regulation of upstream genes. When the expression of *Taed4* and *Yap1* in the same period was detected, we found that *Nat10* depletion did not affect *Tead4* and *Yap1* at the RNA level. Notably, *Nop2-mCherry* increased *Cdx2* and *Gata3* mRNA abundance. In addition, depletion of *Nat10* repressed TEAD4 protein in embryos (Fig. 6b), whereas exogenous *Nop2* RNA partially rescued the level of TEAD4 (Fig. 7g). Overall, the abnormal expression of CDX2 mediated by NOP2 depletion may be caused by the translation obstruction of TEAD4.

Taken together, the above data suggest that NAT10-mediated ac^{4}C modification is involved in the first cell fate decision and affects blastocyst formation in mice by maintaining *Nop2* mRNA expression.

Discussion

Ac^{4}C has been a topic of interest in the study of epigenetic modifications in recent years, thanks to the continuing development of high-throughput sequencing technologies for identifying RNA modifications [34–36]. As a unique RNA acetylation modification event, ac^{4}C is catalyzed by NAT10 and involved in RNA stability and protein translation efficiency in humans [12]. Although the role of ac^{4}C in the occurrence, development, and diagnosis of illnesses, especially cancer, has attracted extensive attention [16–18], its underlying function in other biological processes remains unclear. In mice, ac^{4}C is critical for the growth and maturation of oocytes [19, 20, 37], but its effect on preimplantation embryonic development has not been demonstrated. In this study, we provide convincing evidence of the contribution of NAT10-mediated ac^{4}C to blastocyst formation and maintenance.

RNA-seq combined with RIP-seq is the preferred strategy for investigating genes involved in RNA modification [38, 39]. However, except for a few research groups that could detect nanogram-level RNA [40, 41], ordinary RIP often requires tens to hundreds of micrograms of total RNA [42, 43], making it difficult to perform RIP-seq on preimplantation embryos. Fortunately, PACES and XG-ac4C software are convenient for predicting the ac^{4}C modification motif of human genes [44, 45], and also provide a reference for related research in other species. Based on the results of RNA-seq and acRIP-PCR, as well as research related to preimplantation embryonic development in mice [22], *Nop2* was screened as a candidate target gene regulated by *Nat10*. Relevant studies have demonstrated that embryos with *Nop2* depletion exhibit more severe developmental defects than

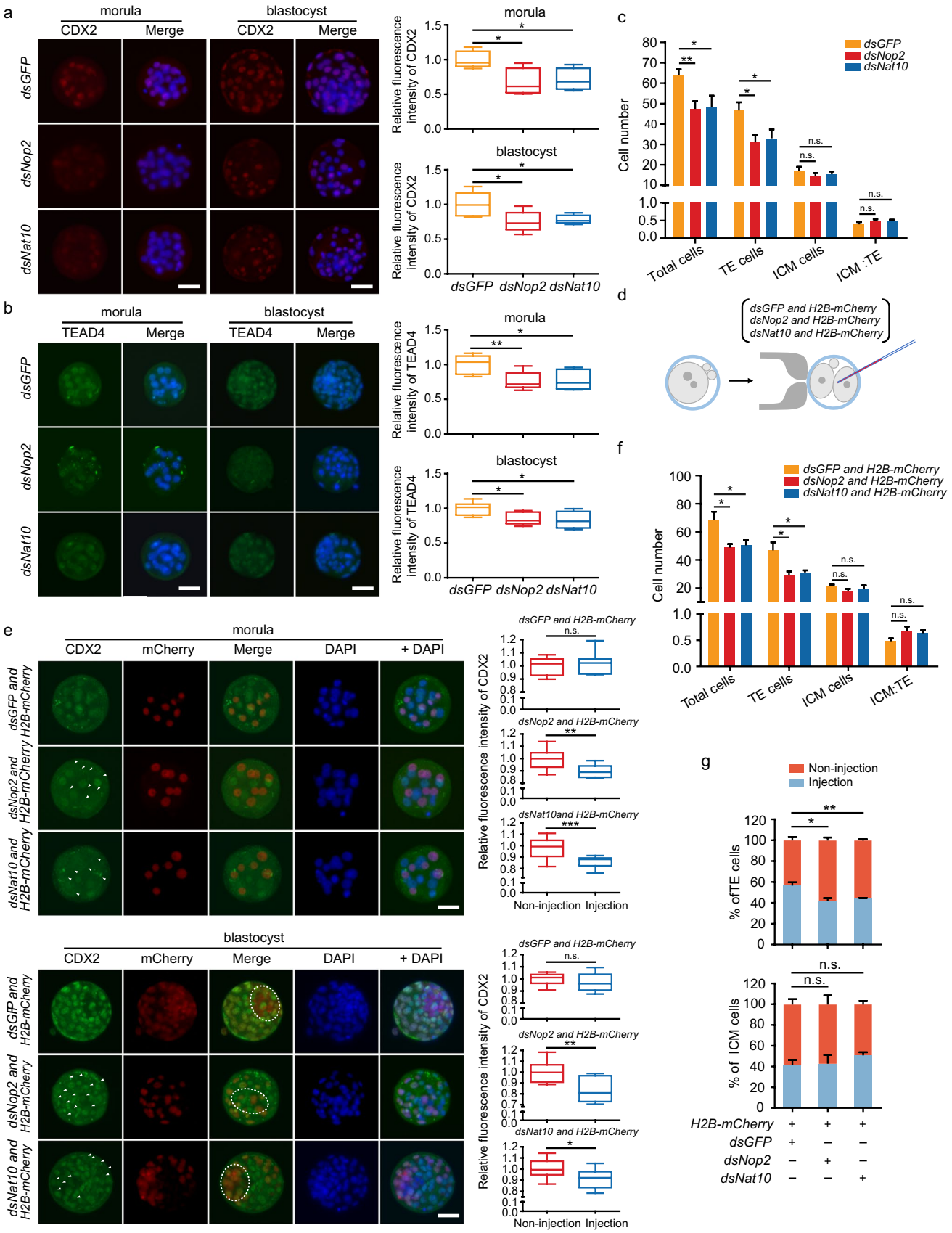
a
morula
blastocyst
CDX2
Merge
dsGFP
dsNop2
dsNat10
Relative fluorescence intensity of CDX2
dsGFP dsNop2 dsNat10
b
TEAD4
Relative fluorescence intensity of TEAD4
c
Cell number
Total cells
TE cells
ICM cells
ICM :TE
n.s.
d
dsGFP and H2B-mCherry
dsNop2 and H2B-mCherry
dsNat10 and H2B-mCherry
f
ICM:TE
e
mCherry
DAPI
+ DAPI
Non-injection
Injection
g
% ofTE cells
% of ICM cells
H2B-mCherry
dsGFP
dsNop2
dsNat10

◂**Fig. 6** *Nop2* depletion mediated by NAT10 knockdown affects the first cell fate decision. **a**, **b** Immunofluorescence analysis of CDX2 (**a**) and TEAD4 (**b**) in morulae and blastocysts derived from zygotes injected with *dsGFP*, *dsNop2*, or *dsNat10* ($n=15$ for morula, $n=20$ for blastocyst). Scale bar, 50 μm. **c** The numbers of total, TE, and ICM cells in blastocysts derived from zygotes injected with dsRNA ($n=20$ for each group). **d** Schematic overview. RNA mixture (*dsGFP* and *H2B-mCherry*, *dsNop2* and *H2B-mCherry*, or *dsNat10* and *H2B-mCherry*) was injected randomly into single blastomeres of 2-cell embryos, and the distribution of mCherry- and CDX2-positive blastomeres was analyzed at the morula and the blastocyst stages. **e** Immunofluorescence analysis of CDX2 (green) and mCherry (red) in morulae (top, $n=15$) and blastocysts (bottom, $n=20$) prepared according to schematic (**d**). Scale bar, 50 μm. White arrowheads denote blastomeres with reduced expression of CDX2 after injection with *dsNat10* or *dsNop2*. White dotted lines indicate ICM. **f** The numbers of total, TE, and ICM cells in blastocysts (n = 20) prepared according to schematic (**d**). **g** Percentage of cells derived from blastomeres that were not injected or injected with RNA mixture (*dsGFP* and *H2B-mCherry*, *dsNop2* and *H2B-mCherry*, or *dsNat10* and *H2B-mCherry*) in the TE (top) and ICM (bottom) cells. *Nat10* or *Nop2* depletion significantly reduced the contribution of blastomeres to TE, but hardly affected the contribution to ICM. For (**a**, **b**, and **e**), boxplots showing the relative fluorescence intensity of CDX2 (**a**, **e**) and TEAD4 (**b**) from three biological replicates, and the mean fluorescence intensity was measured and normalized to the mean fluorescence intensity in *dsGFP*-injected embryos (**a**, **b**) or non-injection blastomeres (**e**). The middle lines indicate the median, and the boxes indicate the $25^{th}/75^{th}$ percentiles. For **c**, **f**, and **g**, error bars represent the SEM in three biological replicates. *P* values were determined by one-way ANOVA (**a-c**, **f**, **g**) or two-sided Student's *t*-test (**e**). $*P<0.05$; $**P<0.01$; $***P<0.001$; *n.s.* no significance

those with *Nat10* depletion, whereby nearly all embryos are arrested at the morula stage [46, 47], which can be explained by the fact that *Nat10*-depleted embryos still have a negligible amount of *Nop2* expression. In addition, NOP2 shows catalytic activity for RNA 5-methylcytosine, but the requirement for NOP2 in mammalian preimplantation embryos is independent of methyltransferase activity [47].

We noticed that the reduction of ac^4C modification on *Nop2* mRNA caused by *Nat10* depletion influenced the first cell fate decision and decreased the abundance of CDX2 in blastomeres, prompting us to reconsider whether NAT10 might hinder preimplantation embryonic development by directly regulating the ac^4C modification of *Cdx2* mRNA. RT-PCR and prediction of ac^4C modification sites confirmed our hypothesis to some degree, however, consistent with previous research [30], *Cdx2* depletion is not the direct cause of blastocyst formation inhibition (Fig. S6c, d). As genes that are closely related to TE development, *Gata3* and *Cdx2* are both regulated by the transcription factor TEAD4 and the transcriptional co-activator YAP1 [48–50]. In this study, *Cdx2* and *Gata3* mRNA was downregulated in *Nat10*- or *Nop2*-depleted morulae, whereas *Tead4* and *Yap1* were not affected. Wang et al. demonstrated that the expression of *Cdx2* was suppressed in *Nop2*-depleted mouse 8-cell embryos, and while the *Tead4* mRNA level did not change, the protein abundance of TEAD4 was significantly reduced; in addition, neither mRNA level nor protein expression and localization of YAP1 were altered [47]. Therefore, the reduction of CDX2 may be caused by the abnormal formation of TEAD4 protein due to the decreased modification of ac^4C in *Nop2* mRNA, which is also confirmed by subsequent experiments.

mRNA completes the conversion of RNA to protein by binding with ribosomes, and NOP2, as an assembly factor, participates in the assembly of the 60S subunit in eukaryotic ribosomes [51, 52]. The differential expression of lineage-specific genes in mice begins at the morula stage [33], and we found that the cellular localization of NOP2 in morula and blastocyst was differed from that in the 2-cell to 8-cell stages, suggesting that NOP2 may play a critical role in the first lineage differentiation of preimplantation embryos. Theoretically, the effect of NOP2 on protein abundance is global, but OCT4 is normally expressed in *Nop2*-depleted morulae [47]. Other functional proteins may be able to substitute NOP2 during ribosomal 60S subunit assembly; on the other hand, NOP2 may have a specific influence on TEAD4 biosynthesis, although this hypothesis requires additional verification.

Tead4$^{-/-}$ embryos failed to develop into normal cavitary blastocysts [32, 50], which explains why most *Nat10*-depleted preimplantation embryos are arrested at the morula stage. Despite the underlying mechanism has not yet been definitively determined, studies have confirmed that the abnormal development of *Tead4*$^{-/-}$ embryos is not directly related to cell proliferation, cell polarity, or adherens junctions [32]. In addition, a few *Nat10*-depleted embryos were able to develop into blastocysts in this study, but with reduced CDX2 abundance and altered cell fate.

Although the expression of *Cdx2* mRNA and protein in mouse preimplantation embryos is still controversial, previous studies have provided a fair description of the regulatory role of CDX2 [30, 31, 53]. As an essential transcription factor for TE development, CDX2 is involved in the regulation of TE formation and maintenance [30, 54, 55]. Here, *Nat10* depletion reduced the expression of *Cdx2* by affecting RNA production, resulting in a significant downregulation of CDX2 protein abundance in morulae and blastocysts. It explains why *Nat10* depletion significantly reduced the number of TE cells in blastocysts. However, the role of NAT10 is extensive, and the decrease in CDX2 expression is only one of the abnormalities in *Nat10*-depleted blastocysts. Therefore, the developmental potential of blastomeres injected with the mixture of *dsNat10* and *H2B-mCherry* may be worse than expected, resulting in the embryo failing to develop into blastocysts or blastocoel cavity collapsing quickly. Furthermore, the expression of *Cdx2* influences the contribution of blastomere to cell lineage by promoting symmetrical division[55]. Hence, the blastomeres injected with *dsNat10* tend to have an asymmetrical division

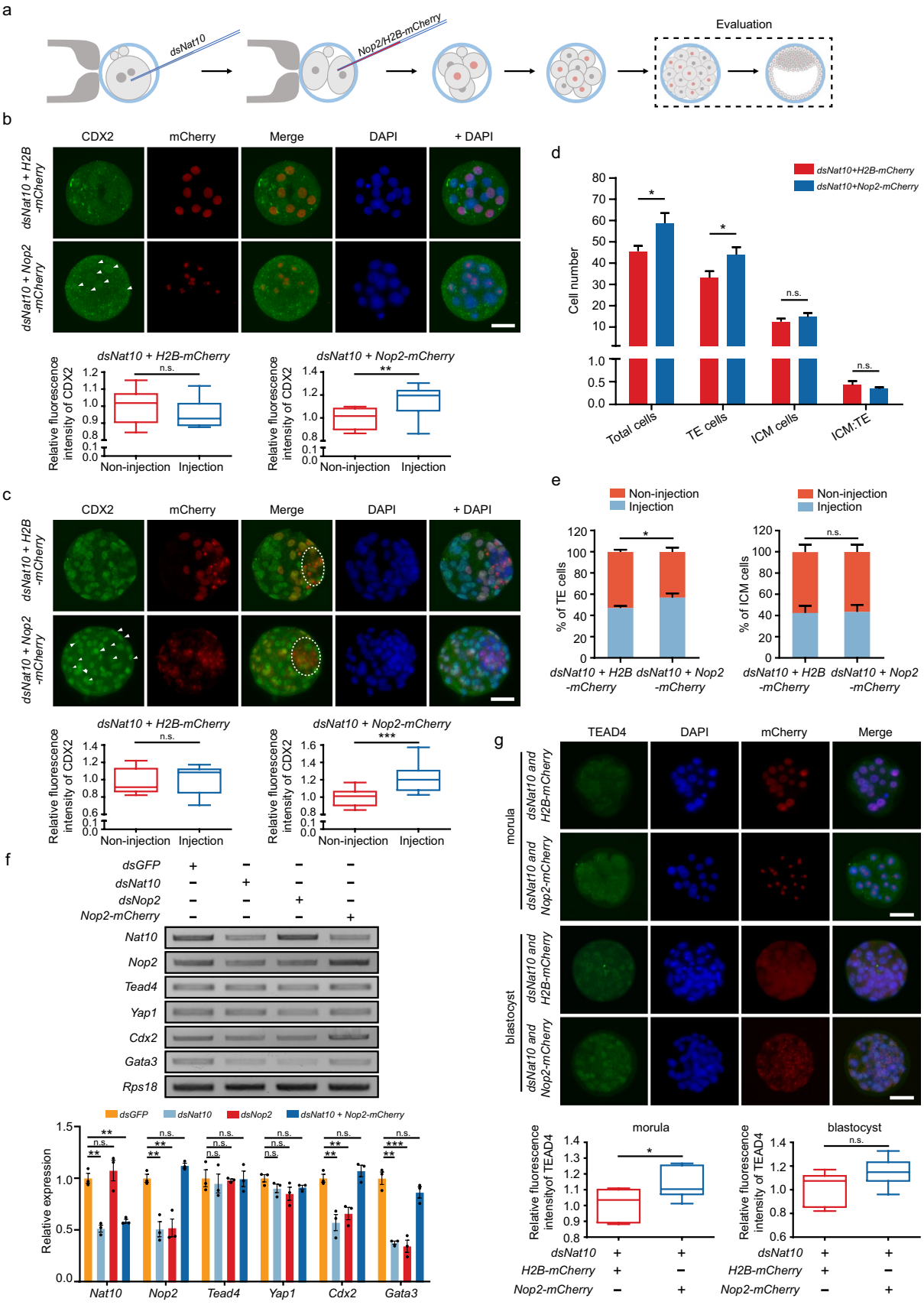
a
dsNat10
Nop2/H2B-mCherry
Evaluation
b
CDX2
mCherry
Merge
DAPI
+ DAPI
dsNat10 + H2B -mCherry
dsNat10 + Nop2 -mCherry
dsNat10 + H2B-mCherry
dsNat10 + Nop2-mCherry
Relative fluorescence intensity of CDX2
n.s.
**
Non-injection
Injection
c
CDX2
mCherry
Merge
DAPI
+ DAPI
dsNat10 + H2B -mCherry
dsNat10 + Nop2 -mCherry
dsNat10 + H2B-mCherry
dsNat10 + Nop2-mCherry
Relative fluorescence intensity of CDX2
n.s.
***
Non-injection
Injection
d
dsNat10+H2B-mCherry
dsNat10+Nop2-mCherry
Cell number
*
n.s.
Total cells
TE cells
ICM cells
ICM:TE
e
Non-injection
Injection
% of TE cells
% of ICM cells
*
n.s.
dsNat10 + H2B -mCherry
dsNat10 + Nop2 -mCherry
f
dsGFP
dsNat10
dsNop2
Nop2-mCherry
Nat10
Nop2
Tead4
Yap1
Cdx2
Gata3
Rps18
dsGFP
dsNat10
dsNop2
dsNat10 + Nop2-mCherry
Relative expression
g
TEAD4
DAPI
mCherry
Merge
morula
blastocyst
dsNat10 and H2B-mCherry
dsNat10 and Nop2-mCherry
morula
blastocyst
Relative fluorescence intensityof TEAD4
*
n.s.
dsNat10
H2B-mCherry
Nop2-mCherry

◂**Fig. 7** Exogenous *Nop2* increases the contribution of *Nat10*-depleted blastomeres to TE. **a** Schematic overview. The cytoplasm of zygotes was first injected with *dsNat10*, then *H2B-* or *Nop2-mCherry* was injected into either blastomere after embryos developed to the 2-cell stage. The distribution of mCherry- and CDX2-positive blastomeres was analyzed at the morula and the blastocyst stages. **b**, **c** Immunofluorescence analysis of CDX2 (green) and mCherry (red) in morulae (**b**, n = 15) and blastocyst (**c**, n = 20) prepared according to schematic (**a**). Scale bar, 50 μm. White arrowheads show that *Nop2* RNA increased the expression of Cdx2 in *Nat10*-depleted blastomeres (**b**, **c**). White dotted lines indicate ICM (**c**). **d** The numbers of total, TE, and ICM cells in blastocysts derived from embryos subjected to two microinjections ($n = 20$). **e** Percentage of cells derived from blastomeres that were not injected or injected with *H2B-/Nop2-mCherry* in the TE (left) and ICM (right) cells. Exogenous *Nop2* significantly increased the contribution of *Nat10*-depleted blastomeres to TE, but hardly affected the contribution to ICM. **f** RT-PCR analysis of *Nat10*, *Nop2*, *Tead4*, *Yap1*, *Cdx2*, and *Gata3* expression in morulae derived from zygotes injected with *dsGFP*, *dsNat10*, *dsNop2*, or *dsNat10* + *Nop2-mCherry*. Bar charts showing the relative expression of genes, which were normalized to the expression of *Rps18*. **g** Immunofluorescence analysis of TEAD4 (green) in morulae and blastocysts derived from zygotes injected with the mixture of *dsNat10* and *H2B-mCherry* or *dsNat10* and *Nop2-mCherry* ($n = 15$ for each group). Exogenous *Nop2* increased the TEAD4 protein abundance in *Nat10*-depleted embryos, especially at the morula stage. Scale bar, 50 μm. For **b**, **c**, and **g**, boxplots showing the relative fluorescence intensity of CDX2 (**b**, **c**) and TEAD4 (**g**) in blastomeres from three biological replicates. The mean fluorescence intensity was measured and normalized to the mean fluorescence intensity in non-injection blastomeres (**b**, **c**) or *dsNat10* + *H2B-mCherry* embryos (**g**). The middle lines indicate the median, and the boxes indicate the 25th/75th percentiles. For **d-f**, error bars represented the SEM in three biological replicates. *P* values were determined by one-way ANOVA (**f**) or two-sided Student's *t*-test (**b-e**, **g**). $^*P < 0.05$; $^{**}P < 0.01$; $^{***}P < 0.001$; *n.s.* no significance

pattern, resulting in a significant reduction in the proportion of blastomeres that eventually develop into TE. Exogenous *Nop2* RNA improves the developmental potential of *Nat10*-depleted blastomeres by increasing CDX2 expression.

In summary, we characterize RNA acetylation modification during preimplantation embryonic development in mice and demonstrate that NAT10-mediated ac^{4}C of *Nop2* mRNA is essential for blastocyst formation and maintenance by influencing the first cell fate decision. These findings serve as an important complement to what is known about the regulation of mammalian embryonic development by ac^{4}C modification and provide a new theoretical basis for further elucidating the biological role of mRNA acetylation modification.

Supplementary Information The online version contains supplementary material available at https://doi.org/10.1007/s00018-023-04955-w.

Author contributions Conceptualization, MYW and QW; Methodology, HJH and ZBH; Validation, ZBH; Formal Analysis, RC and YZ; Investigation, MYW, HJH and QW; Writing—Original Draft, MYW, RC and HJH; Writing—Review & Editing, MYW, HJH, YZ and QW; Visualization, MYW and RC; Funding Acquisition, YZ and QW. All authors discussed the results and approved the final manuscript.

Funding This work was supported by grants from the National Natural Science Foundation of China (31771601, U20A20376, 61972116) and the Applied Technology Research and Development Project of Heilongjiang (GA20C018).

Data Availability All data supporting this study are available within the article and the Supplementary Materials. The RNA-seq data of *Nat10*-depleted morulae in mice have been deposited in the Gene Expression Omnibus database (GEO) under the accession number GSE236943.

Declarations

Conflict of Interest The authors declare that they have no competing interests.

Ethical approval All operations on experimental animals were carried out in accordance with the Guide for the Care and Use of Laboratory Animals from the Harbin Institute of Technology (HIT) and approved by the Institutional Animal Care and Use Committee or Animal Experimental Ethics Committee of HIT (IACUC-2023001).

References

1. Watson AJ, Natale DR, Barcroft LC (2004) Molecular regulation of blastocyst formation. Anim Reprod Sci 82–83:583–592
2. Fleming TP, Pickering SJ (1985) Maturation and polarization of the endocytotic system in outside blastomeres during mouse preimplantation development. J Embryol Exp Morphol 89:175–208
3. Johnson MH, McConnell JM (2004) Lineage allocation and cell polarity during mouse embryogenesis. Semin Cell Dev Biol 15:583–597
4. Johnson MH, Ziomek CA (1983) Cell interactions influence the fate of mouse blastomeres undergoing the transition from the 16- to the 32-cell stage. Dev Biol 95:211–218
5. Dahl JA, Jung I, Aanes H et al (2016) Broad histone h3k4me3 domains in mouse oocytes modulate maternal-to-zygotic transition. Nature 537:548–552
6. Inoue A, Zhang Y (2011) Replication-dependent loss of 5-hydroxymethylcytosine in mouse preimplantation embryos. Science 334:194
7. Sui X, Hu Y, Ren C et al (2020) Mettl3-mediated m(6)a is required for murine oocyte maturation and maternal-to-zygotic transition. Cell Cycle 19:391–404
8. Yang Y, Wang L, Han X et al (2019) Rna 5-methylcytosine facilitates the maternal-to-zygotic transition by preventing maternal mrna decay. Mol Cell 75(1188–1202):e1111
9. Cohn WE (1960) Pseudouridine, a carbon-carbon linked ribonucleoside in ribonucleic acids: Isolation, structure, and chemical characteristics. J Biol Chem 235:1488–1498
10. Kumbhar BV, Kamble AD, Sonawane KD (2013) Conformational preferences of modified nucleoside n(4)-acetylcytidine, ac4c occur at "wobble" 34th position in the anticodon loop of trna. Cell Biochem Biophys 66:797–816
11. Ito S, Horikawa S, Suzuki T et al (2014) Human nat10 is an atp-dependent rna acetyltransferase responsible for n4-acetylcytidine formation in 18 s ribosomal rna (rrna). J Biol Chem 289:35724–35730
12. Arango D, Sturgill D, Alhusaini N et al (2018) Acetylation of cytidine in mrna promotes translation efficiency. Cell 175(1872–1886):e1824

13. Tardu M, Jones JD, Kennedy RT et al (2019) Identification and quantification of modified nucleosides in saccharomyces cerevisiae mrnas. ACS Chem Biol 14:1403–1409
14. Yang W, Li HY, Wu YF et al (2021) Ac4c acetylation of runx2 catalyzed by nat10 spurs osteogenesis of bmscs and prevents ovariectomy-induced bone loss. Mol Ther Nucleic acids 26:135–147
15. Guo G, Shi X, Wang H et al (2020) Epitranscriptomic n4-acetylcytidine profiling in cd4(+) t cells of systemic lupus erythematosus. Front Cell Dev Biol 8:842
16. Zhang Y, Jing Y, Wang Y et al (2021) Nat10 promotes gastric cancer metastasis via n4-acetylated col5a1. Signal Transduct Target Ther 6:173
17. Wang G, Zhang M, Zhang Y et al (2022) Nat10-mediated mrna n4-acetylcytidine modification promotes bladder cancer progression. Clin Transl Med 12:e738
18. Wang K, Zhou LY, Liu F et al (2022) Piwi-interacting rna haapir regulates cardiomyocyte death after myocardial infarction by promoting nat10-mediated ac(4) c acetylation of tfec mrna. Adv Sci 9:e2106058
19. Xiang Y, Zhou C, Zeng Y et al (2021) Nat10-mediated n4-acetylcytidine of rna contributes to post-transcriptional regulation of mouse oocyte maturation in vitro. Front Cell Dev Biol 9:704341
20. Lin J, Xiang Y, Huang J et al (2022) Nat10 maintains oga mrna stability through ac4c modification in regulating oocyte maturation. Front Endocrinol 13:907286
21. Chen L, Wang WJ, Liu Q et al (2022) Nat10-mediated n4-acetylcytidine modification is required for meiosis entry and progression in male germ cells. Nucleic acids Res 50:10896–10913
22. Cui W, Dai X, Marcho C et al (2016) Towards functional annotation of the preimplantation transcriptome: an rnai screen in mammalian embryos. Sci Rep 6:37396
23. Wang Y, Yuan P, Yan Z et al (2021) Single-cell multiomics sequencing reveals the functional regulatory landscape of early embryos. Nat Commun 12:1247
24. Hao Y, Hao S, Andersen-Nissen E et al (2021) Integrated analysis of multimodal single-cell data. Cell 184(3573–3587):e3529
25. Zhou Y, Zhou B, Pache L et al (2019) Metascape provides a biologist-oriented resource for the analysis of systems-level datasets. Nat Commun 10:1523
26. Arango D, Sturgill D, Oberdoerffer S (2019) Immunoprecipitation and sequencing of acetylated rna. Bio-Protoc 9:e3278
27. Chen CY, Ezzeddine N, Shyu AB (2008) Messenger rna half-life measurements in mammalian cells. Methods Enzymol 448:335–357
28. Wang X, Lu Z, Gomez A et al (2014) N6-methyladenosine-dependent regulation of messenger rna stability. Nature 505:117–120
29. Lasman L, Krupalnik V, Viukov S et al (2020) Context-dependent functional compensation between ythdf m(6)a reader proteins. Genes Dev 34:1373–1391
30. Strumpf D, Mao CA, Yamanaka Y et al (2005) Cdx2 is required for correct cell fate specification and differentiation of trophectoderm in the mouse blastocyst. Development 132:2093–2102
31. Jedrusik A, Bruce AW, Tan MH et al (2010) Maternally and zygotically provided cdx2 have novel and critical roles for early development of the mouse embryo. Dev Biol 344:66–78
32. Nishioka N, Yamamoto S, Kiyonari H et al (2008) Tead4 is required for specification of trophectoderm in pre-implantation mouse embryos. Mech Dev 125:270–283
33. Nishioka N, Inoue K, Adachi K et al (2009) The hippo signaling pathway components lats and yap pattern tead4 activity to distinguish mouse trophectoderm from inner cell mass. Dev Cell 16:398–410
34. Sas-Chen A, Thomas JM, Matzov D et al (2020) Dynamic rna acetylation revealed by quantitative cross-evolutionary mapping. Nature 583:638–643
35. Thalalla Gamage S, Sas-Chen A, Schwartz S et al (2021) Quantitative nucleotide resolution profiling of rna cytidine acetylation by ac4c-seq. Nat Protoc 16:2286–2307
36. Arango D, Sturgill D, Yang R et al (2022) Direct epitranscriptomic regulation of mammalian translation initiation through n4-acetylcytidine. Mol Cell 82(2797–2814):e2711
37. Jiang X, Cheng Y, Zhu Y et al (2023) Maternal nat10 orchestrates oocyte meiotic cell-cycle progression and maturation in mice. Nat Commun 14:3729
38. Wu R, Li A, Sun B et al (2019) A novel m(6)a reader prrc2a controls oligodendroglial specification and myelination. Cell Res 29:23–41
39. Lan T, Li H, Zhang D et al (2019) Kiaa1429 contributes to liver cancer progression through n6-methyladenosine-dependent post-transcriptional modification of gata3. Mol Cancer 18:186
40. Wu Y, Xu X, Qi M et al (2022) N(6)-methyladenosine regulates maternal rna maintenance in oocytes and timely rna decay during mouse maternal-to-zygotic transition. Nat Cell Biol 24:917–927
41. Zeng Y, Wang S, Gao S et al (2018) Refined rip-seq protocol for epitranscriptome analysis with low input materials. PLoS Biol 16:e2006092
42. Dominissini D, Moshitch-Moshkovitz S, Salmon-Divon M et al (2013) Transcriptome-wide mapping of n(6)-methyladenosine by m(6)a-seq based on immunocapturing and massively parallel sequencing. Nat Protoc 8:176–189
43. Zhu Z, Xing X, Huang S et al (2021) Nat10 promotes osteogenic differentiation of mesenchymal stem cells by mediating n4-acetylcytidine modification of gremlin 1. Stem Cells Int 2021:8833527
44. Zhao W, Zhou Y, Cui Q et al (2019) Paces: Prediction of n4-acetylcytidine (ac4c) modification sites in mrna. Sci Rep 9:11112
45. Alam W, Tayara H, Chong KT (2020) Xg-ac4c: Identification of n4-acetylcytidine (ac4c) in mrna using extreme gradient boosting with electron-ion interaction pseudopotentials. Sci Rep 10:20942
46. Cui W, Pizzollo J, Han Z et al (2016) Nop2 is required for mammalian preimplantation development. Mol Reprod Dev 83:124–131
47. Wang H, Wang L, Wang Z et al (2020) The nucleolar protein nop2 is required for nucleolar maturation and ribosome biogenesis during preimplantation development in mammals. FASEB J 34:2715–2729
48. Ralston A, Cox BJ, Nishioka N et al (2010) Gata3 regulates trophoblast development downstream of tead4 and in parallel to cdx2. Development 137:395–403
49. Hansen CG, Moroishi T, Guan KL (2015) Yap and taz: a nexus for hippo signaling and beyond. Trends Cell Biol 25:499–513
50. Yagi R, Kohn MJ, Karavanova I et al (2007) Transcription factor tead4 specifies the trophectoderm lineage at the beginning of mammalian development. Development 134:3827–3836
51. Hong B, Brockenbrough JS, Wu P et al (1997) Nop2p is required for pre-rrna processing and 60s ribosome subunit synthesis in yeast. Mol Cell Biol 17:378–388
52. Klinge S, Woolford JL Jr (2019) Ribosome assembly coming into focus. Nat Rev Mol Cell Biol 20:116–131
53. Ralston A, Rossant J (2008) Cdx2 acts downstream of cell polarization to cell-autonomously promote trophectoderm fate in the early mouse embryo. Dev Biol 313:614–629
54. Niwa H, Toyooka Y, Shimosato D et al (2005) Interaction between oct3/4 and cdx2 determines trophectoderm differentiation. Cell 123:917–929
55. Jedrusik A, Parfitt DE, Guo G et al (2008) Role of cdx2 and cell polarity in cell allocation and specification of trophectoderm and inner cell mass in the mouse embryo. Genes Dev 22:2692–2706